EPJ Quantum Technology
a SpringerOpen Journal

RESEARCH   **Open Access**

Check for updates

Demonstration of strong coupling of a subradiant atom array to a cavity vacuum

Bence Gábor[1,2], Adwaith K. Varooli[1,3], Dániel Varga[1,4], Bálint Sárközi[1], Árpád Kurkó[1], András Dombi[1], Thomas W. Clark[1], Francis I.B. Williams[1], David Nagy[1*], András Vukics[1] and Peter Domokos[1]

*Correspondence:
nagy.david@wigner.hun-ren.hu
[1]HUN-REN Wigner RCP, P.O. Box 49,
H-1525 Budapest, Hungary
Full list of author information is
available at the end of the article

Abstract

By considering linear scattering of laser-driven cold atoms inside an undriven high-finesse optical resonator, we experimentally demonstrate effects unique to a strongly coupled vacuum field. Arranging the atoms in an incommensurate lattice with respect to the radiation wavelength, the Bragg scattering into the cavity can be suppressed by destructive interference: the atomic array is subradiant to the cavity mode under transverse illumination. We show however, that strong collective coupling leads to a drastic modification of the excitation spectrum, as evidenced by well-resolved vacuum Rabi splitting in the intensity of the fluctuations. Furthermore, we demonstrate a significant polarization rotation in the linear scattering off the subradiant array via Raman scattering induced by the strongly coupled vacuum field.

Keywords: Cavity quantum electrodynamics; Cold atoms; Subradiant scattering; Vacuum Rabi splitting

1 Introduction

Beyond the peculiar emission from collective Dicke-states of an ensemble of indistinguishable atoms [1], the concept of superradiance [2–5] and subradiance [6–8] has recently been extended to ordered atom arrays [9, 10] in which the interplay of the resonant dipole-dipole interaction together with a constructive or destructive spatial interference leads to enhancement, or inhibition of spontaneous emission, respectively. The latter has application in long-term storage of quantum information [11–13]. Accordingly, there has been an extensive study of regular one-, two-, and three-dimensional atomic arrays, e.g., subradiance has been shown to correspond to optical guided polariton modes in the atomic array [14]. Besides ordering atoms, the radiation can also be shaped to favour emission into selected output channels, such as when coupling them to fibre-guided modes [15–17]. Confinement of the electromagnetic field to waveguides or resonators also results in a spatial enhancement of the range of radiative atom-atom interactions, reinforcing the formation of collective states of an atomic ensemble. Subradiant configurations have been experimentally demonstrated for a one-dimensional array near a waveguide [18].

In this paper, we revisit low-intensity light scattering from a one-dimensional atom array, when the scattered output is directed into strongly coupled radiation modes sustained by
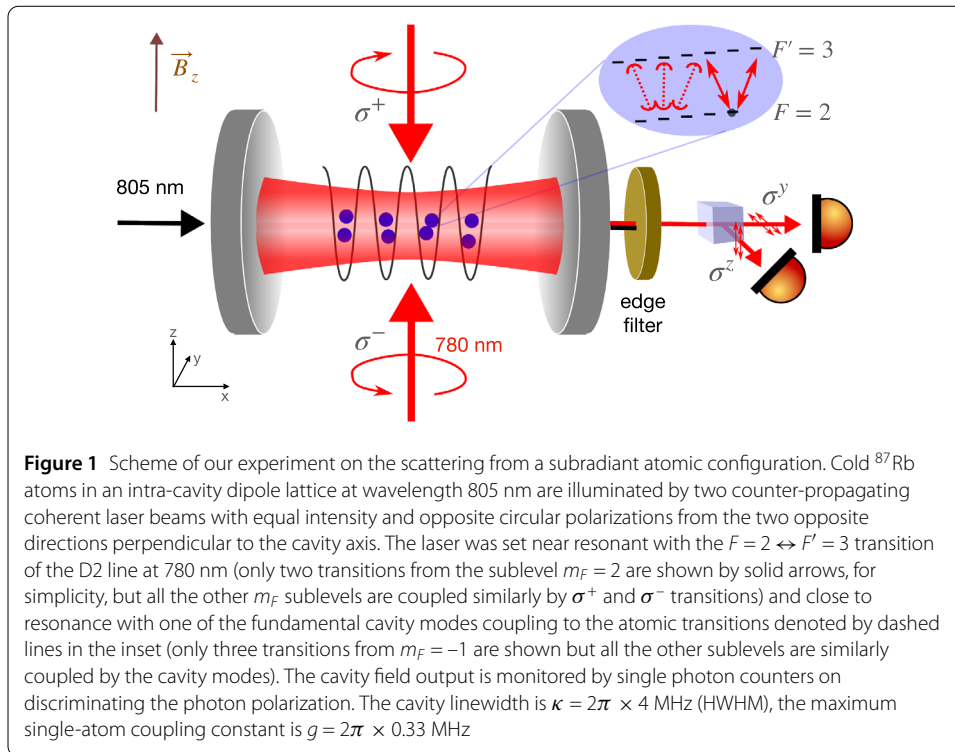
an optical resonator [19, 20]. Dynamics of laser-driven atoms interacting with cavity field modes is of high interest producing a great variety of effects: experiments started with efficient cooling schemes [21], atomic self-organization [22–24] and led to the exploration of superradiant [25–27] and other types of quantum phase transitions [28–38]. Collective radiation effects in many-atom cavity QED systems have been explored, such as the interference in Rayleigh scattering with controlled positioning of atoms in a cavity mode [19, 20, 39–41], quantum non-demolition measurements [42], as well as lasing [43, 44] and superradiant lasing [45–47] with cold atoms as the gain media.

We explore the spectral and polarization properties of scattering from a cold atomic ensemble into a quasi-resonant mode of a high-finesse optical cavity. The atoms are arranged into an optical lattice with periodicity incommensurate with the wavelength of the cavity mode resonating with the driven atomic transition. When they are illuminated from a direction perpendicular to the cavity axis, the coherent Bragg scattering from the atom array is suppressed into the cavity. However, destructive interference does not entail a decoupling from the cavity field even if the laser-driven atom array is without the Bragg condition. There is a collective strong coupling between the subradiant array and the cavity mode, which is manifested by vacuum Rabi splitting [48–51] in the frequency dependence of the outcoupled cavity field intensity fluctuations. We observe another remarkable effect unusual in the fluorescence of atoms in the low-saturation limit: the field polarization is rotated. In coherent Rayleigh scattering, the dipole oscillation of an atom is parallel with the polarization of the impinging field; hence, the scattered field preserves this polarization. This component is, however, suppressed by the destructive interference in the atom array subradiant to the cavity field. The incoherent scattering is enhanced in a high-finesse cavity also into the mode with polarization orthogonal to that of the incoming field. The polarization rotation is associated with a two-photon Raman transition in the atomic hyperfine ground state manifold in accordance with the conservation of angular momentum [26, 52, 53]. We show that this process is on the same order of the drive power and reflects the same vacuum Rabi split spectrum as the polarization-preserving scattering.

2 Results

The experimental scheme is sketched in Fig. 1. Rubidium atoms were trapped in an 805 nm optical lattice sustained by a resonantly driven TEM_{00} mode of a high finesse optical cavity [54]. Another, undriven, fundamental mode of bare cavity resonance frequency ω_C, was set to resonance with the $F = 2 \leftrightarrow F' = 3$ atomic excitation frequency ω_A. The weak probe laser beam, of frequency ω was swept over about ± 50 MHz around ω_A, and illuminates the atoms from a direction perpendicular to the cavity axis. The common detuning $\Delta = \Delta_A = \Delta_C$ where $\Delta_A \equiv \omega - \omega_A$ and $\Delta_C = \omega - \omega_C$. Two single photon counters record separately the cavity output for vertical (z) and horizontal (y) linear polarizations.

Cavity photons in the mode with frequency $\omega_C \approx \omega$ could be generated only by scattering from the laser drive beams. Since the atomic distribution had a periodicity incommensurate with the wavelength of the drive (780 nm), the scattered coherent wave components from different positions of the mode average out along the cavity axis [20, 55]. Quantum emitters can be prepared in subradiant states such that the collective emission amplitude is deterministically canceled out, as seen in perfectly ordered atomic arrays [56] or pure Bose-Einstein condensates. In the present case, the atoms have a finite thermal motion

Figure 1 Scheme of our experiment on the scattering from a subradiant atomic configuration. Cold ^{87}Rb atoms in an intra-cavity dipole lattice at wavelength 805 nm are illuminated by two counter-propagating coherent laser beams with equal intensity and opposite circular polarizations from the two opposite directions perpendicular to the cavity axis. The laser was set near resonant with the $F = 2 \leftrightarrow F' = 3$ transition of the D2 line at 780 nm (only two transitions from the sublevel $m_F = 2$ are shown by solid arrows, for simplicity, but all the other m_F sublevels are coupled similarly by σ^+ and σ^- transitions) and close to resonance with one of the fundamental cavity modes coupling to the atomic transitions denoted by dashed lines in the inset (only three transitions from $m_F = -1$ are shown but all the other sublevels are similarly coupled by the cavity modes). The cavity field output is monitored by single photon counters on discriminating the photon polarization. The cavity linewidth is $\kappa = 2\pi \times 4$ MHz (HWHM), the maximum single-atom coupling constant is $g = 2\pi \times 0.33$ MHz

along the cavity axis around the trap centers. Therefore, suppression of the collective coherent scattering into the cavity is expected only on average over a large statistical ensemble. In each individual measurement, density fluctuations in the half wavelength 805 nm lattice order lead to cavity field fluctuations that are monitored in the outcoupled field by the photodetectors.

2.1 Vacuum Rabi splitting

To start, the number of atoms loaded into the mode volume was varied in the range of ~ 1500 to $\sim 10^4$ by setting different MOT cycle protocols. The effective atom number N_{eff} was determined from independent measurements: it was calibrated by the cavity transmission of a near resonant weak probe detuned from the atomic transition such that the atoms acted as a dispersive medium. The transverse drive laser intensity was lowered as much as possible so that a reasonable rate of photons, ~ 1000 count/second, scattered by the atoms into the cavity could be detected by the single photon counters well above the background. It was ~ 50 count/second coming from ambient light and the 805 laser, while the intrinsic dark count rate was below 1 count/second for the superconducting nanowire single-photon detector. So different drive power was employed for different atom numbers to get this required level of photo-detection rate. Then, at fixed atom number and corresponding drive intensity, the drive laser detuning Δ was varied in the range of ± 50 MHz to probe the excitation spectrum of the system. Figure 2 presents that the intensity fluctuations reflected the vacuum Rabi splitting for large enough atom number. The observed large variance is intrinsic to the density fluctuations of atoms in a subradiant configuration set by the 805 nm wavelength intra-cavity optical lattice. As there is no perfect destructive interference for the finite-size sample of atoms, there is a field with random amplitude. The shot-to-shot fluctuations of the field intensity was found close to the average, indicat-

Figure 2 Vacuum Rabi splitting with a subradiant array of atoms. The photon count rate in the first 1 ms of exposure time is plotted versus the laser drive detuning Δ for various effective atom numbers N_{eff}. Each point and error bar is obtained from an ensemble of 70 runs assuming log-normal distribution, given that the photon count rate is a priori a non-negative quantity. The maxima of the fitted Lorentzian resonance functions, projected on the bottom plane (orange circles), fit well on a parabola $N_{\text{eff}} = \Delta^2/g_{\text{eff}}^2$ with $g_{\text{eff}} = 2\pi \times 0.26$ MHz, in accordance with the $\sqrt{N_{\text{eff}}}$ dependence known for the collective coupling of a number of N_{eff} atoms to a single cavity mode

Figure 3 Power dependence of the vacuum Rabi splitting spectrum for horizontal (a-d) and vertical (e-h) polarization. In panels (b) and (f), the photon count rate normalized to the laser drive power as a function of the drive frequency is shown for 10, 16, 32, 64, 128 and 256 **µ**W in the subplots from top to bottom. Each point is obtained by averaging 50 runs of 100 **µ**s exposure time, and the statistical variance is represented by the error bars. A sum of four Lorentzian curves is a very good fit on all the measured spectra (see text), shown by solid lines. The photon count rate at the outer two peaks of the fit spectra are shown in panels (c) and (g), whereas the corresponding detunings are shown in panels (d) and (h) (left scale, red and blue crosses for negative and positive detunings, respectively). The linewidths of the vacuum Rabi peaks are also presented in panels (d) and (h) (right scale, dots). There is a constant fit on the linewidth data (dashed lines, red and blue, according to the sign of detuning) and similarly on the peak positions (solid line) evidencing the linear scattering regime for the drive power range below 128 µW. At 256 µW saturation effects can be noticed: the peak heights deviate from the linear dependence, and the splitting between the Rabi peaks is also smaller (Data points from the 256 µW measurement are not included in the fits in (c), (d), (g), (h))

ing chaotic light statistics. The main features of the spectra fit a sum of four Lorentzians (see below at Fig. 3), the outer resonances corresponding to normal mode splitting, the inner ones are relevant only for the smallest atom number. The positions of these outer two Lorentzian peaks projected onto the detuning-atom number plane in Fig. 2 are well described by a parabola reflecting the $\Delta \propto \sqrt{N_{\text{eff}}}$ expected for strong collective coupling.

The coefficient $g_{\text{eff}} \approx 2\pi \times 0.26$ MHz from the fit (with uncertainty $2\pi \times 0.006$ MHz) is in good agreement with the expected value of $2\pi \times 0.225$ MHz which can be obtained by averaging over the atomic population distributed evenly in the $F = 2, m_F$ magnetic sublevels with the corresponding Clebsch-Gordan coefficients. We attribute the 10% deviation to the small but not entirely negligible saturation in the atom number calibration measurement.

2.2 Linear scattering

Analysis of the drive power dependence of the vacuum Rabi splitting confirms that the scattering is in the linear regime. The recorded spectra could be compared to a simple theory based on a linear polarizability model of atoms [57] which assumes that the atomic induced dipole is proportional to the local electric field, $\vec{d} \propto \epsilon_0 \chi(\omega) \vec{E}(\vec{r})$ in the low-excitation limit [58].

In our drive field configuration, the two counterpropagating beams have opposite circular polarizations. The resulting electric field is linearly polarized in a helical pattern along the drive axis 'z', i.e., $\vec{E}(\vec{r}) \| \vec{e}_y \cos kz + \vec{e}_x \sin kz$. Note that the optical resonator does not sustain modes with $\vec{e}_x$ polarization, being the direction of the cavity axis; hence, effectively, only the linear polarization $\vec{e}_y$ couples into the resonator field. Linear scatterers lead then to the intracavity field amplitude for the mode polarized in the direction 'y' [20, 58]

$$\alpha_y = \frac{\eta g \sum_a \cos kx_a \cos kz_a}{(i\Delta_{\text{A}} - \gamma)(i\Delta_{\text{C}} - \kappa) + g^2 \sum_a \cos^2 kx_a} \, , \tag{1}$$

where η is an effective drive amplitude and the summation goes over the atoms indexed by $a = 1 \ldots N$ with positions $\vec{r}_a = (x_a, y_a, z_a)$. The squared modulus of the denominator has two minima which, for our setting of resonance between the atoms and the mode, $\Delta_{\text{A}} = \Delta_{\text{C}} = \Delta$, are at $\Delta = \pm\sqrt{g^2 \sum_a \cos^2 kx_a} \equiv \pm\sqrt{N_{\text{eff}}} g$. The effective atom number is around $N_{\text{eff}} \approx N/2$ for $\overline{\cos^2 kx} = 1/2$. This two-peaked resonance behaviour is responsible for the normal mode splitting shown in Fig. 2. A destructive interference leads to vanishing mean field, $\overline{\alpha}$, which is formally represented by the numerator averaging out over the atomic positions, $\langle \sum_a \cos kx_a \cos kz_a \rangle = 0$. This is the case for a homogeneous distribution, but also for a set of positions $\{x_a\}$ sampling the 805 nm wavelength optical lattice. Even if the mean vanishes, however, there are finite size and thermal fluctuations of the atomic distribution which result in cavity field intensity fluctuations, $\overline{|\Delta \alpha_y|^2} \neq 0$. Considering the atomic positions as random variables, the statistical average gives

$$\left\langle \left| \sum_{a=1}^{N} \cos kx_a \cos kz_a \right|^2 \right\rangle \approx N^\beta / 4 \, , \tag{2}$$

where the power law scaling with the atom number N encapsulates two generic cases, i.e., the uniform random or perfectly ordered distributions, leading to $\beta = 1$ linear or $\beta = 2$ quadratic dependences, respectively. The actual value of the exponent β can be deduced from our measured data and gives information on the atomic distribution. For destructive interference, as in our situation where the distribution of atoms is incommensurate with the 780 nm $\cos kx$ mode function, $\beta = 1$ is expected. $\beta = 2$ would indicate superradiance with perfect constructive interference. The photon count rate is proportional to the intracavity photon number, i.e., the squared modulus of the amplitude in Eq. (1), having a

statistical average that can be obtained by using Eq. (2). In the large vacuum Rabi splitting regime and in leading order of $(\kappa^2 + \gamma^2)/N_{\text{eff}}g^2 \ll 1$, the mean of the intensity fluctuations can be approximated around the peak maxima by the Lorentzian functions

$$\langle |\alpha_y|^2 \rangle \approx \frac{\eta^2 N^{\beta-1}}{8} \left[(\Delta \pm \sqrt{N_{\text{eff}}}\, g)^2 + \left(\frac{\kappa + \gamma}{2} \right)^2 \right]^{-1} . \tag{3}$$

This form of the Rabi splitting peaks can be tested experimentally to verify the linear polarizability model of atoms. Moreover, this is a crucial result because it provides a direct measure of β via the scaling of the peak intensity with the number of atoms N.

Figure 3 shows the detected photo-count rate normalized to the pump power. Solid lines show that a function composed of the sum of four Lorentzian functions is a very good fit to the measured points. The outer two peaks correspond to the vacuum Rabi resonances given by Eq. (3). The inner two (smaller) peaks are due to the multiplett structure of the hyperfine states and are significant in the fit to account for the non-vanishing photo-count rate around zero detuning. These peaks will be studied systematically in a subsequent paper. Here we focus on the outer two peaks, i.e., the measured vacuum Rabi peaks which have three features substantiating the validity of the model Eq. (3). First, their separation is constant in the range of pump powers investigated, c.f. Fig. 3(d). It follows then that no noticeable atomic saturation takes place apart from the strongest drive plotted. As a by-product, this peak separation can be used to calibrate N_{eff}. Second, the peak heights of the curves are proportional to the drive power, η^2, which is shown in Fig. 3(c). Some tendency of shrinking peak separation and decreasing peak height can be observed for the strongest drive plotted (256 µW), which indicates that atomic saturation becomes noticeable at this power. However, in the power range up to 100 µW, the scattering is clearly in the linear regime. Third, the linewidths of the vacuum Rabi peaks are constant and are close to the theoretical value $(\kappa + \gamma)/2 \approx 2\pi \times 3.5$ MHz.

2.3 Subradiant atomic array

Having established the linearity of the scattering with driving power, we investigated the dependence of the photon fluctuations scattered into the cavity as a function of the atom number. It was changed by systematically delaying the switch-on time of the transverse drive laser. The drive power was set to a low value, 16 µW, being in the linear scattering regime. The maximum cavity photon number is estimated to be 0.014 corresponding to a saturation around 1.5%. The registered photo-counts were integrated over only 100 µs, in order to minimize the effects of atom loss and atomic motion. The drive frequency was tuned over the same range as in Fig. 3 so that the full excitation spectrum was recorded. This allowed us (i) to calibrate the atom number from the distance of the peak maxima, and (ii) to determine the peak photo-count rate for the given atom number. At the detunings corresponding to the Rabi resonances, $\Delta = \pm\sqrt{N_{\text{eff}}}\, g$, the photo-count rate was measured by averaging over 100 repetitions and is plotted in Fig. 4. This peak scattering rate can be compared with the theoretical maximum rate at vanishing detuning in the denominator of Eq. (3). The corresponding photo-count rate is

$$\frac{I_{\text{detect}}}{P_{\text{dr}}} = \xi\, \kappa_T \times \frac{1}{8} \frac{3\lambda^2}{2\pi \mathcal{A}_{\text{dr}}} \times \frac{\gamma}{\left(\frac{\kappa+\gamma}{2} \right)^2} \times \frac{1}{\hbar\omega} \approx 6000 \, \frac{\text{counts}}{\text{s} \cdot \mu\text{W}}, \tag{4}$$

Figure 4 Collective scattering as a function of the atom number. The maximum photon scattering rates on resonance with the vacuum Rabi peaks, both at the negative (red) and positive (blue) side of the detuning, have been detected during a time duration of 100 μs at a controlled delay after loading the atoms into the lattice. For each atom number, the drive frequency were set to resonance with the vacuum Rabi peaks. Horizontal and vertical polarizations are summed up. The exponents of the linear fit on the log-log scale are obtained $\beta = 0.875 \pm 0.009$ for the red and $\beta = 0.853 \pm 0.031$ for the blue, respectively

where $\kappa_T = 2\pi \times 1.15$ MHz is the cavity field decay by mirror transmission, $\xi = 0.5$ is the detection efficiency, γ is the atomic linewidth (HWHM), $\mathcal{A}_{\mathrm{dr}}$ is the drive beam cross section, and the drive power P_{dr} is measured in μW. With our experimental parameters, the expected count rate is 96 kHz, which is in acceptable agreement with the measured values in the range 30 ± 3 kHz, shown in Fig. 4, provided we take into account some uncontrolled misalignment of the transverse drive laser and incomplete illumination of the entire atom cloud in the cavity. The measured maximum rates scatter within 10% around a constant value, and show some dependence as a function of atom number, but the power law fit results in an exponent only slightly below 1, which is consistent with $\beta = 1$ in Eq. (3). This confirms the absence of coherent component in the scattered photon field and supports the observation of subradiance from an array of atoms. Beyond a simplified one-dimensional form of subradiance, the cavity does not merely enhance the scattering into a small solid angle for each individual atom, but the collective strong coupling to the cavity mode modifies the excitation spectrum of the atom array.

2.4 Polarization rotation

The strongly coupled vacuum field influences not only the spectral features of scattering but also the polarization. Within the scalar linear polarizability model leading to Eq. (1), the atomic polarization induced by the 'z' travelling $\sigma^{\pm}$ beams excites the 'y' polarized mode of the cavity. This is Rayleigh scattering which corresponds to the resonance fluorescence of two-level atoms in the low-excitation limit. As far as coherent scattering and interference of the scattered light off many atoms is concerned, the linear polarizability approach is suitable. However, the degeneracy of the atomic $F = 2$ ground-state level changes substantially the incoherent scattering. The drive excites $(2, m_F) \rightarrow (3, m_F \pm 1)$ transitions which have dipole moments in the 'y' and 'x' directions. The Rayleigh scattering involves thus $(2, m_F) \leftrightarrow (3, m_F \pm 1)$ atomic transitions within a two-level system, while creating an 'y' polarized photon from the laser drive. The strongly coupled 'z' polarized mode of the cavity, however, even in vacuum state, can stimulate $(3, m_F \pm 1) \rightarrow (2, m_F \pm 1)$ transitions. This is Raman scattering: the initial and final atomic states $(2, m_F)$ and $(2, m_F \pm 1)$, respectively, are different along the excitation path. The change of the angular momentum state

of the atom compensates for the rotation of the field polarization when a 'z' polarized photon is created in the cavity from a field polarized in the (x, y) plane. Another consequence of the change of the atomic state in the Raman scattering process is that the scattered photon carries which-way information; hence the scattered components from different atoms in the ensemble do not interfere. Regardless the position of the atoms, there is no collective enhancement, nor destructive interference, only the intensities from individual sources add up.

The cavity-induced Raman scattering process has been observed by a photon flux emanating from the mode with polarization 'z' (σ_0) which is the direction of propagation of the input field. The scattering rate into the polarization 'z' as a function of the laser drive detuning for a range of drive powers is shown in Fig. 3(f). It shows very similar features and count rates to the 'y' polarization output: (i) vacuum Rabi peaks are linear in the input power (panel (g)) and (ii) constant widths have been measured (panel (h)). The results show that the cavity-stimulated Raman scattering is also linear in the drive intensity in the low-excitation limit. This is at variance with the case of two-level atoms where the incoherent part of the scattered light is connected to saturation and is of quadratic order in the drive intensity. Furthermore, the peak heights were obtained close to those of the polarization-maintaining light scattering, which reinforces the observation that the coherent scattering was strongly suppressed, i.e., another indirect evidence for the subradiance.

The two-photon Raman transition has been exploited to realize quantum interfaces between light polarization and atomic memory states [59, 60] by means of stimulated adiabatic passage processes with pulsed excitation in single-atom strong-coupling cavity QED experiments. Cavity-enhanced Raman scattering has also been observed from a regular half-wavelength ordered array [20] when the drive is detuned from the atoms. In our experiment, we revealed that the Raman scattering, though being an incoherent process, manifests the vacuum Rabi split spectrum characteristic of the strong collective coupling of the atoms to the 'z' polarized cavity mode.

3 Discussion

An important conclusion is that radiation from atomic arrays is not only efficiently collected but is substantially *modified* by the presence of a high-finesse resonator. Most importantly, the strong coupling to selected resonator modes imposes a *collective* scattering from the atoms into the resonator. This collective coupling, as we have shown, is due to more than simply an interference effect, even in the extremely low intensity limit. The role of collective coupling has been revealed in detecting the collective phase shift of Bragg back-scattered light from a one-dimensional optical lattice along the axis of a ring cavity [61]. Here we realized an experiment where the input field impinges on a one-dimensional atom array from a direction perpendicular to the axis of an undriven resonator, and the collective effect is captured by the Rabi splitting in the intensity of fluctuations around a zero mean-field.

A natural continuation of this work consists in the exploration of the non-linear regime arising at increased powers, e.g., the systematic study of the inner two Lorentzian resonances appearing in the measured data. On a longer time scale, our experiment can be developed toward the realization of new variants of the Dicke model [62] in disordered manifolds with cavity-mediated interactions. Further, considering that multiply excited subradiant states are said to be composed of the superposition of singly excited states in

random ensembles [13], our system could be used to provide further insight into this superposition. In particular, our system is well suited for time-resolved measurements and so the dynamics of the underlying subradiant states in the single-mode limit are available.

We must conclude, too, that optical polarization enters the linear scattering regime. On the one hand, the multiple ground-state level structure of atoms has to be taken into account in a linear polarizability description of atoms, beyond the usual scalar polarizability, which was noted as a subtlety in Ref. [14]. On the other hand, the multiple ground states open the possibility of entanglement-based, new type of subradiant states predicted recently [63]. In our future work, the cavity-enhanced polarization rotation could be the design basis for long-range many-body interactions between atoms mediated by two-mode fields. The cavity field fluctuations reflecting a non-trivial atom-cavity spectrum can be exploited as a useful light source when the mean-field is suppressed. Finally, our configuration is very close to schemes for superradiant lasing [46] and for atomic clocks [27] which we hope to explore with the incommensurate lattice trap.

4 Methods

Loading atoms into the cavity　An ensemble of cold ^{87}Rb atoms was collected in a magneto-optical trap (MOT). After the MOT cycle, the atoms were cooled by polarization gradient cooling ($\sigma^+ - \sigma^-$ configuration) down to temperatures of 20–50 µK. Subsequently, they are magnetically polarized by optical pumping into the $(F, m_F) = (2, 2)$ hyperfine ground state to allow capture with a magnetic quadrupole trap. The magnetically trapped atomic cloud was then transported into the mode of a high-finesse ($\mathcal{F}/\pi = 1430$) resonator by adiabatically displacing the trap center, and was released there by turning off the magnetic field in 7 ms.

The cavity is $l = 15$ mm long and the mode waist is $w = 127$ µm. A far red detuned (805 nm) laser beam was injected into the cavity, serving two purposes: firstly, utilizing the Pound-Drever-Hall technique, the cavity was locked to it, secondly, it provided a far-red-detuned optical dipole lattice for the atoms with a depth of 140 µK and an unperturbed lifetime of 200 ms.

Upon the arrival and release of the atoms, a second optical pumping was performed into the $(F, m_F) = (2, 2)$ hyperfine ground state defined by a homogeneous magnetic field of 1G along 'z'. Starting from the initial Zeeman sublevel, the population spreads over all other sublevels and tends to some steady state population distribution as a result of the competition between fluorescence, Raman transitions and repumping from the $F = 1$ level. The actual steady-state distribution in the m_F sublevels is unknown, but it is not very far from a uniform one (Markov chain simulation according to the Clebsch-Gordan coefficients).

For the measurements leading to Fig. 2, the atom number was varied by applying a delay (in the range 8–12 ms, which is safely after the decay of magnetic field transients) before the illumination of the atoms was switched on.

Calibration of the atom number　The effective number of atoms which coupled to the cavity (N_{eff}) was measured from the light shift effect. In the dispersive limit, where $\Delta_A \gg \gamma$, the atoms shift the cavity mode resonance proportional to their number. The laser drive, resonant with the empty cavity mode, was set to $\omega - \omega_A = \Delta_A = -2\pi \times 90$ MHz detuning from the atomic resonance, hence the corresponding total dispersive frequency shift was

$N_{\text{eff}} g^2/\Delta_A$, that was determined directly from a transmission measurement. The effective number N_{eff} includes the reduced coupling strength g away from the axis following a Gaussian transverse mode profile (which effect is the same for the transverse drive configuration), and the averaging over the mode function $\cos(kx)$ along the cavity axis.

Transverse drive   This laser was phase-locked to a reference laser with a variable detuning from the atomic resonance, which we scanned in the frequency range ± 30 MHz. The beam waist was 1 mm, the power in each direction was adjusted from 0.15 µW to 256 µW by means of an acousto-optic modulator (AOM). Simultaneously, the $F = 1 \leftrightarrow F' = 2$ transition was also driven resonantly by a repumper laser, in order to keep the atoms in the $F = 2 \leftrightarrow F' = 3$ cycle. The beam waist of the repumper was 12 mm, the power in each direction was 4 mW.

Detection   The 805 nm component was removed by interference filters from the cavity output beam which was then split by a polarizing beam splitter. Both the horizontal and vertical polarization beams were coupled into a fibre, connected to a superconducting nanowire single-photon detector (for the measurements shown in Fig. 2) or to a single photon counter module (for the measurements shown in Fig. 3 and Fig. 4). The overall detection efficiency was 7% and 50%, respectively, including the quantum efficiency and the optical coupling into the detector. Although the superconducting nanowire single photon detector has a very high quantum efficiency ($> 99\%$), the photon loss was significant during the optical path from the cavity output to the detector including several fibre couplings. Altogether the total efficiency was low (7%), therefore we decided to install a new detection system with 65% quantum efficiency detectors but with very high optical coupling (finally we reached 50% overall detection efficiency). We recorded few millisecond long signals with time resolution 1 µs.

Shot-to-shot noise in the atom number   In the experiment the averaging over many realizations may involve a random variation of the atom number. On taking this into account, the Eq. (3) is modified and the peak intensity scaling on resonance gets a correction:

$$S_{\max}(\Delta_{\text{peak}}) = \frac{4\eta^2 N^{\beta-1}}{(\kappa + \gamma)^2} \left(1 - \frac{4g^2}{(\kappa + \gamma)^2} \frac{\delta N^2}{\bar{N}} \right) , \tag{5}$$

where δN is the variance around the mean $\bar{N}$. The correction is, however, small for the sub-Poissonian atom number statistics in our MOT.

Data availability
No datasets were generated or analysed during the current study.

Declarations

Competing interests
The authors declare no competing interests.

Author details
[1]HUN-REN Wigner RCP, P.O. Box 49, H-1525 Budapest, Hungary. [2]Department of Theoretical Physics, University of Szeged, Tisza Lajos körút 84, H-6720 Szeged, Hungary. [3]Université Paris-Saclay, CNRS, ENS Paris-Saclay, CentraleSupélec, LuMIn, 91190 Gif-sur-Yvette, France. [4]Department of Physics of Complex Systems, ELTE Eötvös Loránd University, Pázmány Péter sétány 1/A, H-1117 Budapest, Hungary.

References

1. Gross M, Haroche S. Superradiance: an essay on the theory of collective spontaneous emission. Phys Rep. 1982;93(5):301–96. https://doi.org/10.1016/0370-1573(82)90102-8.
2. DeVoe RG, Brewer RG. Observation of superradiant and subradiant spontaneous emission of two trapped ions. Phys Rev Lett. 1996;76(12):2049–52. https://doi.org/10.1103/PhysRevLett.76.2049.
3. Inouye S, Chikkatur AP, Stamper-Kurn DM, Stenger J, Pritchard DE, Ketterle W. Superradiant Rayleigh scattering from a Bose-Einstein condensate. Science. 1999;285:571–4.
4. Araújo MO, Krešić I, Kaiser R, Guerin W. Superradiance in a large and dilute cloud of cold atoms in the linear-optics regime. Phys Rev Lett. 2016;117(7):073002. https://doi.org/10.1103/PhysRevLett.117.073002.
5. Ferioli G, Glicenstein A, Ferrier-Barbut I, Browaeys A. A non-equilibrium superradiant phase transition in free space. Nat Phys. 2023;19(9):1345–9. https://doi.org/10.1038/s41567-023-02064-w.
6. Guerin W, Araújo MO, Kaiser R. Subradiance in a large cloud of cold atoms. Phys Rev Lett. 2016;116(8):083601. https://doi.org/10.1103/PhysRevLett.116.083601.
7. Das D, Lemberger B, Yavuz DD. Subradiance and superradiance-to-subradiance transition in dilute atomic clouds. Phys Rev A. 2020;102(4):043708. https://doi.org/10.1103/PhysRevA.102.043708.
8. Rui J, Wei D, Rubio-Abadal A, Hollerith S, Zeiher J, Stamper-Kurn DM, Gross C, Bloch I. A subradiant optical mirror formed by a single structured atomic layer. Nature. 2020;583(7816):369–74. https://doi.org/10.1038/s41586-020-2463-x.
9. Zoubi H, Ritsch H. Excitons and cavity polaritons for optical lattice ultracold atoms. In: Advances in atomic, molecular, and optical physics. vol. 62. Amsterdam: Elsevier; 2013. p. 171–229. https://doi.org/10.1016/B978-0-12-408090-4.00003-7. https://linkinghub.elsevier.com/retrieve/pii/B9780124080904000037. Accessed 2024-07-18.
10. Bettles RJ, Gardiner SA, Adams CS. Enhanced optical cross section via collective coupling of atomic dipoles in a 2d array. Phys Rev Lett. 2016;116:103602. https://doi.org/10.1103/PhysRevLett.116.103602.
11. Plankensteiner D, Ostermann L, Ritsch H, Genes C. Selective protected state preparation of coupled dissipative quantum emitters. Sci Rep. 2015;5(1):16231. https://doi.org/10.1038/srep16231.
12. Facchinetti G, Jenkins SD, Ruostekoski J. Storing light with subradiant correlations in arrays of atoms. Phys Rev Lett. 2016;117(24):243601. https://doi.org/10.1103/PhysRevLett.117.243601.
13. Ferioli G, Glicenstein A, Henriet L, Ferrier-Barbut I, Browaeys A. Storage and release of subradiant excitations in a dense atomic cloud. Phys Rev X. 2021;11(2):021031. https://doi.org/10.1103/PhysRevX.11.021031.
14. Asenjo-Garcia A, Moreno-Cardoner M, Albrecht A, Kimble HJ, Chang DE. Exponential improvement in photon storage fidelities using subradiance and "selective radiance" in atomic arrays. Phys Rev X. 2017;7(3):031024. https://doi.org/10.1103/PhysRevX.7.031024.
15. Solano P, Barberis-Blostein P, Fatemi FK, Orozco LA, Rolston SL. Super-radiance reveals infinite-range dipole interactions through a nanofiber. Nat Commun. 2017;8(1):1857. https://doi.org/10.1038/s41467-017-01994-3.
16. Albrecht A, Henriet L, Asenjo-Garcia A, Dieterle PB, Painter O, Chang DE. Subradiant states of quantum bits coupled to a one-dimensional waveguide. New J Phys. 2019;21(2):025003. https://doi.org/10.1088/1367-2630/ab0134.
17. Pennetta R, Lechner D, Blaha M, Rauschenbeutel A, Schneeweiss P, Volz J. Observation of coherent coupling between super- and subradiant states of an ensemble of cold atoms collectively coupled to a single propagating optical mode. Phys Rev Lett. 2022;128:203601. https://doi.org/10.1103/PhysRevLett.128.203601.
18. Loo AF, Fedorov A, Lalumière K, Sanders BC, Blais A, Wallraff A. Photon-mediated interactions between distant artificial atoms. Science. 2013;342:1494–6.
19. Reimann R, Alt W, Kampschulte T, Macha T, Ratschbacher L, Thau N, Yoon S, Meschede D. Cavity-modified collective Rayleigh scattering of two atoms. Phys Rev Lett. 2015;114(2):023601. https://doi.org/10.1103/PhysRevLett.114.023601.
20. Yan Z, Ho J, Lu Y-H, Masson SJ, Asenjo-Garcia A, Stamper-Kurn DM. Superradiant and subradiant cavity scattering by atom arrays. Phys Rev Lett. 2023;131(25):253603. https://doi.org/10.1103/PhysRevLett.131.253603.
21. Nussmann S, Hijlkema M, Weber B, Rohde F, Rempe G, Kuhn A. Submicron positioning of single atoms in a microcavity. Phys Rev Lett. 2005;95:173602.
22. Domokos P, Ritsch H. Collective cooling and self-organization of atoms in a cavity. Phys Rev Lett. 2002;89:253003.
23. Black AT, Chan HW, Vuletić V. Observation of collective friction forces due to spatial self-organization of atoms: from Rayleigh to Bragg scattering. Phys Rev Lett. 2003;91:203001.
24. Arnold KJ, Baden MP, Barrett MD. Self-organization threshold scaling for thermal atoms coupled to a cavity. Phys Rev Lett. 2012;109(15):153002. https://doi.org/10.1103/PhysRevLett.109.153002.
25. Slama S, Krenz G, Bux S, Zimmermann C, Courteille PW. Cavity-enhanced superradiant Rayleigh scattering with ultracold and Bose-Einstein condensed atoms. Phys Rev A. 2007;75:063620.
26. Zhang Z, Lee CH, Kumar R, Arnold KJ, Masson SJ, Grimsmo AL, Parkins AS, Barrett MD. Dicke-model simulation via cavity-assisted Raman transitions. Phys Rev A. 2018;97(4):043858. https://doi.org/10.1103/PhysRevA.97.043858.
27. Bohr EA, Kristensen SL, Hotter C, Schäffer SA, Robinson-Tait J, Thomsen JW, Zelevinsky T, Ritsch H, Müller JH. Collectively enhanced Ramsey readout by cavity sub- to superradiant transition. Nat Commun. 2024;15(1):1084. https://doi.org/10.1038/s41467-024-45420-x.

28. Baumann K, Guerlin C, Brennecke F, Esslinger T. Dicke quantum phase transition with a superfluid gas in an optical cavity. Nature. 2010;464:1301–6.
29. Landig R, Hruby L, Dogra N, Landini M, Mottl R, Donner T, Esslinger T. Quantum phases from competing short- and long-range interactions in an optical lattice. Nature. 2016;532:476–9.
30. Léonard J, Morales A, Zupancic P, Esslinger T, Donner T. Supersolid formation in a quantum gas breaking a continuous translational symmetry. Nature. 2017;543(7643):87–90. https://doi.org/10.1038/nature21067.
31. Klinder J, Keßler H, Bakhtiari MR, Thorwart M, Hemmerich A. Observation of a superradiant Mott insulator in the Dicke-Hubbard model. Phys Rev Lett. 2015;115:230403.
32. Kollár AJ, Papageorge AT, Vaidya VD, Guo Y, Keeling J, Lev BL. Supermode-density-wave-polariton condensation with a Bose–Einstein condensate in a multimode cavity. Nat Commun. 2017;8(1):14386. https://doi.org/10.1038/ncomms14386.
33. Muniz JA, Barberena D, Lewis-Swan RJ, Young DJ, Cline JRK, Rey AM, Thompson JK. Exploring dynamical phase transitions with cold atoms in an optical cavity. Nature. 2020;580(7805):602–7. https://doi.org/10.1038/s41586-020-2224-x.
34. Keßler H, Kongkhambut P, Georges C, Mathey L, Cosme JG, Hemmerich A. Observation of a dissipative time crystal. Phys Rev Lett. 2021;127(4):043602. https://doi.org/10.1103/PhysRevLett.127.043602.
35. Mivehvar F, Piazza F, Donner T, Ritsch H. Cavity QED with quantum gases: new paradigms in many-body physics. Adv Phys. 2021;70(1):1–153. https://doi.org/10.1080/00018732.2021.1969727.
36. Clark TW, Dombi A, Williams FIB, Kurkó A, Fortágh J, Nagy D, Vukics A, Domokos P. Time-resolved observation of a dynamical phase transition with atoms in a cavity. Phys Rev A. 2022;105:063712. https://doi.org/10.1103/PhysRevA.105.063712.
37. Gábor B, Nagy D, Dombi A, Clark TW, Williams FIB, Adwaith KV, Vukics A, Domokos P. Ground-state bistability of cold atoms in a cavity. Phys Rev A. 2023;107:023713. https://doi.org/10.1103/PhysRevA.107.023713.
38. Helson V, Zwettler T, Mivehvar F, Colella E, Roux K, Konishi H, Ritsch H, Brantut J-P. Density-wave ordering in a unitary Fermi gas with photon-mediated interactions. Nature. 2023;618(7966):716–20. https://doi.org/10.1038/s41586-023-06018-3.
39. Casabone B, Friebe K, Brandstätter B, Schüppert K, Blatt R, Northup TE. Enhanced quantum interface with collective ion-cavity coupling. Phys Rev Lett. 2015;114(2):023602. https://doi.org/10.1103/PhysRevLett.114.023602.
40. Neuzner A, Körber M, Morin O, Ritter S, Rempe G. Interference and dynamics of light from a distance-controlled atom pair in an optical cavity. Nat Photonics. 2016;10(5):303–6. https://doi.org/10.1038/nphoton.2016.19.
41. Hotter C, Ostermann L, Ritsch H. Cavity sub- and superradiance for transversely driven atomic ensembles. Phys Rev Res. 2023;5(1):013056. https://doi.org/10.1103/PhysRevResearch.5.013056.
42. Mekhov IB, Ritsch H. Quantum nondemolition measurements and state preparation in quantum gases by light detection. Phys Rev Lett. 2009;102:020403.
43. Guerin W, Michaud F, Kaiser R. Mechanisms for lasing with cold atoms as the gain medium. Phys Rev Lett. 2008;101(9):093002. https://doi.org/10.1103/PhysRevLett.101.093002.
44. Sawant R, Rangwala SA. Lasing by driven atoms-cavity system in collective strong coupling regime. Sci Rep. 2017;7(1):11432. https://doi.org/10.1038/s41598-017-11799-5.
45. Meiser D, Holland MJ. Steady-state superradiance with alkaline-Earth-metal atoms. Phys Rev A. 2010;81(3):033847. https://doi.org/10.1103/PhysRevA.81.033847.
46. Bohnet JG, Chen Z, Weiner JM, Meiser D, Holland MJ, Thompson JK. A steady-state superradiant laser with less than one intracavity photon. Nature. 2012;484(7392):78–81. https://doi.org/10.1038/nature10920.
47. Norcia MA, Winchester MN, Cline JRK, Thompson JK. Superradiance on the millihertz linewidth strontium clock transition. Sci Adv. 2016;2(10):1601231. https://doi.org/10.1126/sciadv.1601231.
48. Thompson RJ, Rempe G, Kimble HJ. Observation of normal-mode splitting for an atom in an optical cavity. Phys Rev Lett. 1992;68:1132–5.
49. Tuchman AK, Long R, Vrijsen G, Boudet J, Lee J, Kasevich MA. Normal-mode splitting with large collective cooperativity. Phys Rev A. 2006;74(5):053821. https://doi.org/10.1103/PhysRevA.74.053821.
50. Hernandez G, Zhang J, Zhu Y. Vacuum Rabi splitting and intracavity dark state in a cavity-atom system. Phys Rev A. 2007;76(5):053814. https://doi.org/10.1103/PhysRevA.76.053814.
51. Courteille PW, Rivero D, Franca GH, Pessoa CA, Cipris A, Portela M, Teixeira RC, Slama S. Photonic bands and normal mode splitting in optical lattices interacting with cavities. Phys Rev A. 2025;111:013310. https://doi.org/10.1103/PhysRevA.111.013310.
52. Vrijsen G, Hosten O, Lee J, Bernon S, Kasevich MA. Raman lasing with a cold atom gain medium in a high-finesse optical cavity. Phys Rev Lett. 2011;107(6):063904. https://doi.org/10.1103/PhysRevLett.107.063904.
53. Suarez E, Carollo F, Lesanovsky I, Olmos B, Courteille PW, Slama S. Collective atom-cavity coupling and nonlinear dynamics with atoms with multilevel ground states. Phys Rev A. 2023;107(2):023714. https://doi.org/10.1103/PhysRevA.107.023714.
54. Varga D, Gábor B, Sárközi B, Adwaith KV, Nagy D, Dombi A, Clark TW, Williams FIB, Domokos P, Vukics A. Loading atoms from a large magnetic trap to a small intra-cavity optical lattice. Phys Lett A. 2024;505:129444. https://doi.org/10.1016/j.physleta.2024.129444.
55. Zippilli S, Morigi G, Ritsch H. Suppression of Bragg scattering by collective interference of spatially ordered atoms with a high-Q cavity mode. Phys Rev Lett. 2004;93(12):123002. https://doi.org/10.1103/PhysRevLett.93.123002.
56. Mekhov IB, Maschler C, Ritsch H. Cavity-enhanced light scattering in optical lattices to probe atomic quantum statistics. Phys Rev Lett. 2007;98:100402. https://doi.org/10.1103/PhysRevLett.98.100402.
57. Tanji-Suzuki H, Leroux ID, Schleier-Smith MH, Cetina M, Grier AT, Simon J, Vuletic V. Interaction Between Atomic Ensembles and Optical Resonators: classical Description. 2011. http://arxiv.org/abs/1104.3594.
58. Ritsch H, Domokos P, Brennecke F, Esslinger T. Cold atoms in cavity-generated dynamical optical potentials. Rev Mod Phys. 2013;85:553–601.
59. Wilk T, Webster SC, Kuhn A, Rempe G. Single-atom single-photon quantum interface. Science. 2007;317(5837):488–90. https://doi.org/10.1126/science.1143835.
60. Specht HP, Nölleke C, Reiserer A, Uphoff M, Figueroa E, Ritter S, Rempe G. A single-atom quantum memory. Nature. 2011;473(7346):190–3. https://doi.org/10.1038/nature09997.

61. Slama S, Cube C, Deh B, Ludewig A, Zimmermann C, Courteille PW. Phase-sensitive detection of Bragg scattering at 1d optical lattices. Phys Rev Lett. 2005;94:193901. https://doi.org/10.1103/PhysRevLett.94.193901.
62. Zhiqiang Z, Lee CH, Kumar R, Arnold KJ, Masson SJ, Parkins AS, Barrett MD. Nonequilibrium phase transition in a spin-1 Dicke model. Optica. 2017;4(4):424. https://doi.org/10.1364/OPTICA.4.000424.
63. Hebenstreit M, Kraus B, Ostermann L, Ritsch H. Subradiance via entanglement in atoms with several independent decay channels. Phys Rev Lett. 2017;118(14):143602. https://doi.org/10.1103/PhysRevLett.118.143602.

Publisher's note

Springer Nature remains neutral with regard to jurisdictional claims in published maps and institutional affiliations.